Scattering from Two-dimensional Inhomogeneous Periodic Dielectric Layer above a Stratified Dielectric Medium [1]

Problem of scattering from periodic surfaces can be viewed, in the most general configuration, as the problem of scattering from an inhomogeneous dielectric slab with an arbitrary one-dimensional periodic permittivity profile above a half-space stratified medium. In a simple case of two homogeneous media with non-planar periodic interface, the periodic interface can be inscribed between two parallel planar boundaries to form an inhomogeneous periodic dielectric slab between the two media. In this section we seek a numerical solution for the total field (or polarization current) inside the periodic inhomogeneous layer lying over a stratified dielectric half-space illuminated by a plane wave. The geometry of the scattering problem is shown in Fig. 1. First the two-dimensional Green's function for a stratified dielectric medium is found. Using Floquet's theorem these results are extended to the periodic case. Then the problem will be formulated as an integral equation that can be solved numerically by the method of moments.

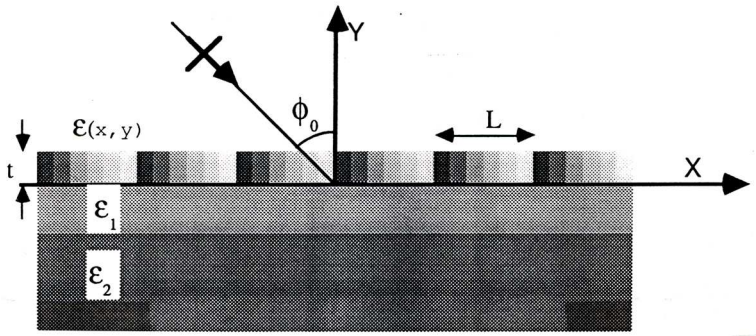

Figure 1: Geometry of a periodic inhomogeneous dielectric layer over a stratified dielectric half-space.

1 Two-dimensional Green's Function for a Stratified Dielectric Half Space

For a volume distribution of electric current ($\boldsymbol{J}_e$) occupying region V in free space, the corresponding Hertz vector is given by (2) and the resulting fields are given by (1) with

[1] Copyright K. Sarabandi, 1997.

$\mathbf{\Pi}_m = 0$. Since in the two-dimensional problems $\frac{\partial}{\partial z} = 0$, from equation (3) the field components in terms of the Hertz vector potential can be expanded as:

$$\begin{aligned} E_x &= k_0^2 \left(1 + \tfrac{1}{k_0^2}\tfrac{\partial^2}{\partial x^2}\right)\Pi_x + \tfrac{\partial^2}{\partial x \partial y}\Pi_y \\ E_y &= \tfrac{\partial^2}{\partial y \partial x}\Pi_x + k_0^2 \left(1 + \tfrac{1}{k_0^2}\tfrac{\partial^2}{\partial y^2}\right)\Pi_y \\ E_z &= k_0^2 \Pi_z \end{aligned} \tag{1}$$

The Hertz vector potential associated with an infinite current filament located at point (x', y') in free space with amplitude I_p and orientation $\hat{p}$ is of the form

$$\Pi_p(x, y) = \frac{-Z_0}{4k_0} H_0^{(1)}(k_0\sqrt{(x-x')^2 + (y-y')^2})I_p \qquad p = x, y \text{ or } z. \tag{2}$$

The corresponding field components can be obtained by inserting (2) into (1) and then by employing the identity

$$H_0^{(1)}(k_0\sqrt{(x-x')^2 + (y-y')^2}) = \frac{1}{\pi}\int_{-\infty}^{+\infty} \frac{e^{ik_y|y-y'| - ik_x(x-x')}}{k_y} \mathrm{d}k_x \tag{3}$$

the resulting fields can be expressed in terms of continuous spectrum of plane waves. In (3) $k_y = \sqrt{k_0^2 - k_x^2}$ and the branch of the square root is chosen such that $\sqrt{-1} = i$. In the presence of the dielectric half-space, when the current filament is in the upper half-space, each plane wave, is reflected at the air-dielectric interface according to Fresnel's reflection law. It should be noted that the incidence angle of each plane wave, in general, is complex and is given by

$$\gamma = \arctan(\frac{k_x}{k_y}).$$

The net effect of the dielectric half-space on the radiated field can be obtained by superimposing all of the reflected plane waves that are of the following form

$$R_q(\gamma)e^{ik_y(y+y') - ik_x(x-x')}, \qquad q = E \text{ or } H.$$

where $R_q(\gamma)$ is the Fresnel reflection coefficient. The total reflected field can now be obtained by noting that

$$\begin{aligned} E_x^r &= -R_H(\gamma)E_x^i \\ E_y^r &= R_H(\gamma)E_y^i \\ E_z^r &= R_E(\gamma)E_z^i \end{aligned}$$

and since the direction of propagation along the y axis is reversed for the reflected waves, the operator $\frac{\partial}{\partial y}$ for the x and y components of the reflected field must be replaced by

$-\frac{\partial}{\partial y}$. Thus,

$$\begin{aligned}
E_x^r &= -\tfrac{k_0 Z_0}{4\pi}[-I_x(1+\tfrac{1}{k_0^2}\tfrac{\partial^2}{\partial x^2}) + I_y \tfrac{1}{k_0^2}\tfrac{\partial^2}{\partial x \partial y}] \int_{-\infty}^{+\infty} R_H(\gamma) \tfrac{e^{ik_y(y+y')-ik_x(x-x')}}{k_y} \mathrm{d}k_x, \\
E_y^r &= -\tfrac{k_0 Z_0}{4\pi}[-I_x \tfrac{1}{k_0^2}\tfrac{\partial^2}{\partial y \partial x} + I_y(1+\tfrac{1}{k_0^2}\tfrac{\partial^2}{\partial y^2})] \int_{-\infty}^{+\infty} R_H(\gamma) \tfrac{e^{ik_y(y+y')-ik_x(x-x')}}{k_y} \mathrm{d}k_x, \\
E_z^r &= -\tfrac{k_0 Z_0}{4\pi} I_z \int_{-\infty}^{+\infty} R_E(\gamma) \tfrac{e^{ik_y(y+y')-ik_x(x-x')}}{k_y} \mathrm{d}k_x.
\end{aligned} \tag{4}$$

In matrix notation the total field in the upper half-space can be represented by

$$\boldsymbol{E} = \begin{bmatrix} G_{xx} & G_{xy} & 0 \\ G_{yx} & G_{yy} & 0 \\ 0 & 0 & G_{zz} \end{bmatrix} \begin{bmatrix} I_x \\ I_y \\ I_z \end{bmatrix}, \tag{5}$$

where

$$\begin{aligned}
G_{xx} &= -\tfrac{k_0 Z_0}{4}(1+\tfrac{1}{k_0^2}\tfrac{\partial^2}{\partial x^2})[H_0^{(1)}(k_0\sqrt{(x-x')^2+(y-y')^2}) \\
&\quad -\tfrac{1}{\pi}\int_{-\infty}^{+\infty} R_H(\gamma)\tfrac{e^{ik_y(y+y')-ik_x(x-x')}}{k_y}\mathrm{d}k_x], \\
G_{xy} &= -\tfrac{Z_0}{4k_0}\tfrac{\partial^2}{\partial x \partial y}[H_0^{(1)}(k_0\sqrt{(x-x')^2+(y-y')^2}) \\
&\quad +\tfrac{1}{\pi}\int_{-\infty}^{+\infty} R_H(\gamma)\tfrac{e^{ik_y(y+y')-ik_x(x-x')}}{k_y}\mathrm{d}k_x], \\
G_{yx} &= -\tfrac{Z_0}{4k_0}\tfrac{\partial^2}{\partial y \partial x}[H_0^{(1)}(k_0\sqrt{(x-x')^2+(y-y')^2}) \\
&\quad -\tfrac{1}{\pi}\int_{-\infty}^{+\infty} R_H(\gamma)\tfrac{e^{ik_y(y+y')-ik_x(x-x')}}{k_y}\mathrm{d}k_x], \\
G_{yy} &= -\tfrac{k_0 Z_0}{4}(1+\tfrac{1}{k_0^2}\tfrac{\partial^2}{\partial y^2})[H_0^{(1)}(k_0\sqrt{(x-x')^2+(y-y')^2}) \\
&\quad +\tfrac{1}{\pi}\int_{-\infty}^{+\infty} R_H(\gamma)\tfrac{e^{ik_y(y+y')-ik_x(x-x')}}{k_y}\mathrm{d}k_x], \\
G_{zz} &= -\tfrac{k_0 Z_0}{4}[H_0^{(1)}(k_0\sqrt{(x-x')^2+(y-y')^2}) \\
&\quad +\tfrac{1}{\pi}\int_{-\infty}^{+\infty} R_E(\gamma)\tfrac{e^{ik_y(y+y')-ik_x(x-x')}}{k_y}\mathrm{d}k_x]
\end{aligned} \tag{6}$$

are the elements of the dyadic Green's function for two-dimensional layered dielectric half-space problems. If an electric current distribution $\boldsymbol{J}_e$ occupies region S in the upper half-space, the radiated electric field at any point in the upper half-space can be obtained from:

$$\begin{aligned}
E_x^s(x,y) &= \int_S [G_{xx}(x,y;x',y')J_x(x',y') + G_{xy}(x,y;x',y')J_y(x',y')]\mathrm{d}x'\mathrm{d}y' \\
E_y^s(x,y) &= \int_S [G_{yx}(x,y;x',y')J_x(x',y') + G_{yy}(x,y;x',y')J_y(x',y')]\mathrm{d}x'\mathrm{d}y' \\
E_z^s(x,y) &= \int_S G_{zz}(x,y;x',y')J_z(x',y')\mathrm{d}x'\mathrm{d}y'
\end{aligned} \tag{7}$$

2 Far Field Evaluation

In scattering problems the quantity of interest usually is the far field expression. Here we derive the approximate form of the Green's function in the far zone using the saddle-point technique. All the elements of the dyadic Green's function have an integral of the

form

$$I = \frac{1}{\pi}\int_{-\infty}^{+\infty} R_q(\gamma)\frac{e^{ik_y(y+y')-ik_x(x-x')}}{k_y}\mathrm{d}k_x \tag{8}$$

Using the standard change of variable

$$k_x = k_0 \sin\gamma$$

the integration contour is changed from the real axis in the complex k_x-plane to contour Γ in γ-plane as shown in Fig. 2.

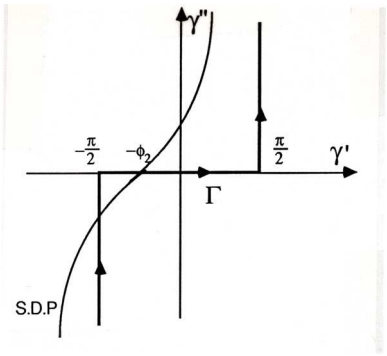

Figure 2: Contour of integration and steepest descent path in γ-plane.

Also by defining

$$x - x' = \rho_2 \sin\phi_2, \qquad y + y' = \rho_2 \cos\phi_2$$

integral (8) in γ-plane becomes:

$$I = \frac{1}{\pi}\int_{\Gamma} R_q(\gamma) e^{ik_0\rho_2\cos(\gamma+\phi_2)}\mathrm{d}\gamma$$

The saddle point is the solution of

$$\frac{\mathrm{d}}{\mathrm{d}\gamma}\cos(\gamma+\phi_2) = 0$$

implies $\gamma = -\phi_2$. When $k_0\rho_2 \gg 1$ the approximate value of I can be obtained by deforming the contour of integration from Γ to the steepest descent path (S.D.P.) given by

$$\mathrm{Im}[i\cos(\gamma+\phi_2)] = 1.$$

There are some poles associated with the reflection coefficient function ($R_q(\gamma)$) of a layered dielectric medium that are captured when the contour is deformed. The contribution of these poles gives rise to surface waves, but their effect can be ignored if the

dielectric materials are lossy and observation point is away from the interface. Under these conditions we get

$$\begin{aligned} I &= \tfrac{1}{\pi} R_q(-\phi_2) \int_{S.D.P.} e^{ik_0\rho_2\cos(\gamma+\phi_2)} \mathrm{d}\gamma \\ &\approx \sqrt{\tfrac{2}{\pi k_0\rho_2}} e^{i(k_0\rho_2-\pi/4)} R_q(\phi_2), \end{aligned}$$

where we have used the fact that R_q is an even function. Also the large argument expansion of the Hankel function can be used for distant approximations, i.e.

$$H_0^{(1)}(k_0\sqrt{(x-x')^2+(y-y')^2}) \approx \sqrt{\frac{2}{\pi k_0\rho_1}} e^{i(k_0\rho_1-\pi/4)},$$

where $\rho_1 = \sqrt{(x-x')^2+(y-y')^2}$. From Fig. 3 it is seen that in the far zone the following approximations can be used also

$$\begin{aligned} &\phi_1 = \phi_2 = \phi, \\ &\rho_1 = \rho - x'\sin\phi - y'\cos\phi, \\ &\rho_2 = \rho - x'\sin\phi + y'\cos\phi. \end{aligned}$$

These approximations can be inserted into expressions for the dyadic Green's function given by (6). The far field approximation of derivatives of the Hankel function and integral I can be obtained by retaining the terms up to the order $\rho^{-1/2}$ and discarding the rest. Thus the expressions for the Green's function elements in the far zone become:

$$\begin{aligned} G_{xx} = &\ -\tfrac{k_0Z_0}{4}\sqrt{\tfrac{2}{\pi k_0\rho}} e^{i(k_0\rho-\pi/4)} \cos^2\phi e^{-ik_0\sin\phi x'}[e^{-ik_0\cos\phi y'} - R_H(\phi)e^{ik_0\cos\phi y'}] \\ G_{xy} = &\ \tfrac{k_0Z_0}{4}\sqrt{\tfrac{2}{\pi k_0\rho}} e^{i(k_0\rho-\pi/4)} \sin\phi\cos\phi e^{-ik_0\sin\phi x'}[e^{-ik_0\cos\phi y'} + R_H(\phi)e^{ik_0\cos\phi y'}] \\ G_{yx} = &\ \tfrac{k_0Z_0}{4}\sqrt{\tfrac{2}{\pi k_0\rho}} e^{i(k_0\rho-\pi/4)} \sin\phi\cos\phi e^{-ik_0\sin\phi x'}[e^{-ik_0\cos\phi y'} - R_H(\phi)e^{ik_0\cos\phi y'}] \\ G_{yy} = &\ -\tfrac{k_0Z_0}{4}\sqrt{\tfrac{2}{\pi k_0\rho}} e^{i(k_0\rho-\pi/4)} \sin^2\phi e^{-ik_0\sin\phi x'}[e^{-ik_0\cos\phi y'} + R_H(\phi)e^{ik_0\cos\phi y'}] \\ G_{zz} = &\ -\tfrac{k_0Z_0}{4}\sqrt{\tfrac{2}{\pi k_0\rho}} e^{i(k_0\rho-\pi/4)} e^{-ik_0\sin\phi x'}[e^{-ik_0\cos\phi y'} + R_E(\phi)e^{ik_0\cos\phi y'}]. \end{aligned} \tag{9}$$

It can easily be shown that for an electric current distribution $\boldsymbol{J}_e$ the radiated far field does not have a $\hat{\rho}$ component and the far field amplitude defined by

$$\boldsymbol{E} = \sqrt{\frac{2}{\pi k_0\rho}} e^{i(k_0\rho-\pi/4)} \boldsymbol{S}$$

has components

$$\begin{aligned} S_\phi = &\ \tfrac{k_0Z_0}{4}\{\textstyle\int_S \cos\phi J_x(x',y') e^{-ik_0\sin\phi x'}[e^{-ik_0\cos\phi y'} - R_H(\phi)e^{ik_0\cos\phi y'}]\mathrm{d}x'\mathrm{d}y' \\ &\ - \textstyle\int_S \sin\phi J_y(x',y') e^{-ik_0\sin\phi x'}[e^{-ik_0\cos\phi y'} + R_H(\phi)e^{ik_0\cos\phi y'}]\mathrm{d}x'\mathrm{d}y'\}, \\ S_z = &\ -\tfrac{k_0Z_0}{4}\textstyle\int_S J_z(x',y') e^{-ik_0\sin\phi x'}[e^{-ik_0\cos\phi y'} + R_E(\phi)e^{ik_0\cos\phi y'}]\mathrm{d}x'\mathrm{d}y', \end{aligned} \tag{10}$$

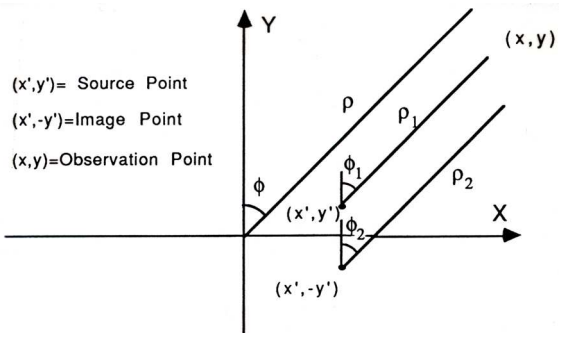

Figure 3: Geometry of the line source and its image.

3 Reflection Coefficient of a Layered Dielectric Half-Space

Consider a multilayer dielectric half-space as shown in Fig. 4. Interface of the m^{th} and $(m+1)^{th}$ layers is located at $y = -d_m$ with $d_0 = 0$. The relative permittivity and permeability of each region is represented by ϵ_m and μ_m respectively. Suppose a plane wave whose plane of incidence is parallel with $x - y$ plane is illuminating the stratified medium from above. From symmetry considerations, $\frac{\partial}{\partial z} = 0$, which implies that the field components in each region can be separated into E- and H-polarized waves. It can be shown from Maxwell's equation that the E- and H-polarized waves are dual of each other, i.e. one can be obtained from the other upon replacing E_m with H_m, H_m with $-E_m$, and $\epsilon_m(\mu_m)$ with $\mu_m(\epsilon_m)$.

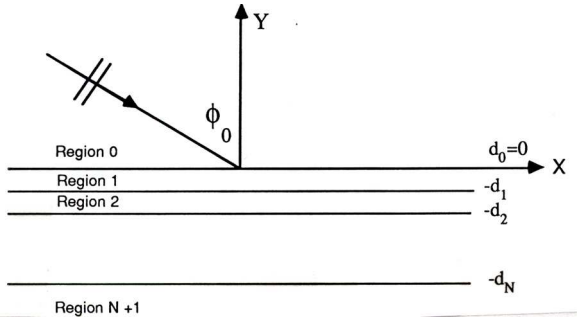

Figure 4: Plane wave reflection from a multi-layer dielectric half-space.

For E polarization the field components in region m can be represented by

$$\begin{aligned} E_{my} &= [c_m^i e^{-ik_{my}y} + c_m^r e^{ik_{my}y}] e^{ik_0 \sin\phi_0 x} \\ H_{mx} &= \tfrac{Y_0 k_{my}}{k_0 \mu_m} [c_m^i e^{-ik_{my}y} - c_m^r e^{ik_{my}y}] e^{ik_0 \sin\phi_0 x} \end{aligned}$$

where ϕ_0 is the incidence angle and $k_{my} = k_0\sqrt{\epsilon_m\mu_m - \sin^2\phi_0}$. The coefficient c_m^i and c_m^r are the amplitude of the wave travelling in the $-z$ and $+z$ direction, respectively,

in region m. In region 0, $c_0^i = 1$, and $c_0^r = R_E$ is the total reflection coefficient and in region $N+1$, which is semi-infinite, $c_{N+1}^r = 0$. Imposing the boundary conditions, which requires continuity tangential electric and magnetic fields at each dielectric interface, we can relate the field amplitudes in the m^{th} to those of $(m+1)^{th}$ region.

After some simple algebraic manipulation, the following recursive relationship can be obtained

$$\frac{c_m^r}{c_m^i} = \frac{(c_{m+1}^r/c_{m+1}^i) + \Gamma_m^E e^{i2k_{(m+1)z}d_m}}{(c_{m+1}^r/c_{m+1}^i)\Gamma_m^E + e^{i2k_{(m+1)z}d_m}} e^{i2k_{my}d_m} \tag{11}$$

where

$$\Gamma_m^E = \frac{\mu_{m+1}k_{my} - \mu_m k_{(m+1)y}}{\mu_{m+1}k_{my} + \mu_m k_{(m+1)y}}.$$

Starting from $c_{N+1}^r/c_{N+1}^i = 0$ and using (11) repeatedly $R_E = c_0^r/c_0^i$ can be found. To find R_H the reflection coefficient for H polarization, the duality relationship can be applied and an identical recursive formulation as given in (11) can be obtained. The only difference is that Γ_m^E becomes Γ_m^H which is given by

$$\Gamma_m^H = \frac{\epsilon_{m+1}k_{my} - \epsilon_m k_{(m+1)y}}{\epsilon_{m+1}k_{my} + \epsilon_m k_{(m+1)y}}.$$

4 Scattering from Inhomogeneous Periodic Dielectric Layer above a Half-Space Layered Medium

Consider an inhomogeneous dielectric layer of thickness t ontop of a stratified half-space dielectric medium as shown in Fig. 1. The permittivity of the inhomogeneous layer is represented by $\epsilon(x, y)$ which is a periodic function of x with period L. Suppose this structure is illuminated by a plane wave whose angle of incidence and polarization respectively are ϕ_0 and $\hat{p}$. For an E-polarized wave $\hat{p} = \hat{z}$ and for an H-polarized wave $\hat{p} = -\cos\phi_0\hat{x} - \sin\phi_0\hat{y}$, thus the incident wave may be represented by

$$\boldsymbol{E}^i = \hat{p}e^{ik_0(\sin\phi_0 x - \cos\phi_0 y)}. \tag{12}$$

A polarization current distribution is induced in the inhomogeneous layer. This current gives rise to a scattered field that can be obtained from (7). The polarization current is proportional to the total field within the inhomogeneous layer. The total field is comprised of the incident field, the reflected field which would have existed in the absence of the inhomogeneous layer, and the scattered field, i.e.

$$\boldsymbol{E}^t = \boldsymbol{E}^i + \boldsymbol{E}^r + \boldsymbol{E}^s.$$

The polarization current in terms of the total field is given by

$$\boldsymbol{J}_e(x,y) = -ik_0 Y_0(\epsilon(x,y)-1)\boldsymbol{E}^t. \tag{13}$$

Upon substitution of expression (7) for $\boldsymbol{E}^s$ into (13) a set of integral equations for polarization current can be obtained; for E polarization we have

$$\begin{aligned} J_z(x,y) = \; & -ik_0 Y_0(\epsilon(x,y)-1)\{e^{ik_0 \sin\phi_0 x}[e^{-ik_0\cos\phi_0 y} + R_E(\phi_0)e^{ik_0\cos\phi_0 y}] \\ & + \textstyle\int_0^t \int_{-\infty}^{+\infty} J_z(x',y')G_{zz}(x,y;x',y')\mathrm{d}x'\mathrm{d}y'\}, \end{aligned} \tag{14}$$

and for H polarization

$$\begin{aligned} J_x(x,y) = \; & -ik_0 Y_0(\epsilon(x,y)-1)\{\cos\phi_0 e^{ik_0\sin\phi_0 x}[-e^{-ik_0\cos\phi_0 y} + R_H(\phi_0)e^{ik_0\cos\phi_0 y}] \\ & + \textstyle\int_0^t \int_{-\infty}^{+\infty}[J_x(x',y')G_{xx}(x,y;x',y') + J_y(x',y')G_{xy}(x,y;x',y')]\mathrm{d}x'\mathrm{d}y'\}, \\ J_y(x,y) = \; & -ik_0 Y_0(\epsilon(x,y)-1)\{-\sin\phi_0 e^{ik_0\sin\phi_0 x}[e^{-ik_0\cos\phi_0 y} + R_H(\phi_0)e^{ik_0\cos\phi_0 y}] \\ & + \textstyle\int_0^t \int_{-\infty}^{+\infty}[J_x(x',y')G_{yx}(x,y;x',y') + J_y(x',y')G_{yy}(x,y;x',y')]\mathrm{d}x'\mathrm{d}y'\}. \end{aligned} \tag{15}$$

Since there is no closed-form representation for the kernel of these integral equations, finding the solution, even numerically, seems impossible. But by employing Floquet's theorem the integral equations can be reduced to a form which is amenable to numerical solution. The fact that the permittivity of the inhomogeneous layer is periodic in x,excluding a phase factor, all the field quantities are required to be periodic in x . Therefore the polarization current must satisfy

$$\boldsymbol{J}_e(x+nL,y) = \boldsymbol{J}_e(x,y)e^{ik_0\sin\phi_0 nL} \tag{16}$$

Now using (16) the integration with respect to x can be simplified significantly by breaking the integral into multiples of a period, that is

$$\begin{aligned} I_{zz} &= \textstyle\int_{-\infty}^{+\infty} G_{zz}(x,y;x',y')J_z(x',y')\mathrm{d}x'\mathrm{d}y' \\ &= \textstyle\sum_{n=-\infty}^{+\infty}\int_{x_0+nL}^{x_0+(n+1)L} G_{zz}(x,y;x',y')J_z(x',y')\mathrm{d}x'\mathrm{d}y' \end{aligned} \tag{17}$$

At this stage, if the variable x' is changed to $x'+nL$ and property (16) is used, I_{zz} becomes

$$I_{zz} = \int_{x_0}^{x_0+L} G_{zz}^p(x,y;x',y')J_z(x',y')\mathrm{d}x'\mathrm{d}y'$$

where

$$G_{zz}^p(x,y;x',y') = \sum_{n=-\infty}^{+\infty} G_{zz}(x,y;x'+nL,y')e^{ik_0\sin\phi_0 nL}$$

If the expression for G_{zz} as given by (6) is inserted in the above equation and the order of summation and integration is interchanged, and then the identity

$$\sum_{n=-\infty}^{+\infty} e^{inL(k_0\sin\phi_0+k_x)} = 2\pi \sum_{n=-\infty}^{+\infty}\delta[(k_x+k_0\sin\phi_0)L - 2\pi n]$$

is employed, the periodic Green's function simplifies to

$$G^p_{zz}(x,y;x',y') = -\frac{k_0 Z_0}{2L}\sum_{n=-\infty}^{+\infty}[e^{ik_{ny}|y-y'|} + R_E(\gamma_n)e^{ik_{ny}(y+y')}]\frac{e^{-ik_{nx}(x-x')}}{k_{ny}} \tag{18}$$

where

$$k_{nx} = \frac{2\pi n}{L} - k_0\sin\phi_0, \qquad k_{ny} = \sqrt{k_0^2 - k_{nx}^2},$$

and

$$\gamma_n = \arctan(\frac{k_{nx}}{k_{ny}}).$$

Other elements of the periodic Green's function can also be obtained in the same manner

$$\begin{aligned}
G^p_{xx}(x,y;x',y') &= -\tfrac{k_0 Z_0}{2L}(1+\tfrac{1}{k_0^2}\tfrac{\partial^2}{\partial x^2})\textstyle\sum_{n=-\infty}^{+\infty}[e^{ik_{ny}|y-y'|} - R_H(\gamma_n)e^{ik_{ny}(y+y')}]\tfrac{e^{-ik_{nx}(x-x')}}{k_{ny}}\\
G^p_{xy}(x,y;x',y') &= -\tfrac{Z_0}{2Lk_0}\tfrac{\partial^2}{\partial x\partial y}\textstyle\sum_{n=-\infty}^{+\infty}[e^{ik_{ny}|y-y'|} + R_H(\gamma_n)e^{ik_{ny}(y+y')}]\tfrac{e^{-ik_{nx}(x-x')}}{k_{ny}}\\
G^p_{yx}(x,y;x',y') &= -\tfrac{Z_0}{2Lk_0}\tfrac{\partial^2}{\partial y\partial x}\textstyle\sum_{n=-\infty}^{+\infty}[e^{ik_{ny}|y-y'|} - R_H(\gamma_n)e^{ik_{ny}(y+y')}]\tfrac{e^{-ik_{nx}(x-x')}}{k_{ny}}\\
G^p_{yy}(x,y;x',y') &= -\tfrac{k_0 Z_0}{2L}(1+\tfrac{1}{k_0^2}\tfrac{\partial^2}{\partial y^2})\textstyle\sum_{n=-\infty}^{+\infty}[e^{ik_{ny}|y-y'|} + R_H(\gamma_n)e^{ik_{ny}(y+y')}]\tfrac{e^{-ik_{nx}(x-x')}}{k_{ny}}.
\end{aligned} \tag{19}$$

The integral equations (14) and (15) now take the following form

$$\begin{aligned}
J_z(x,y) = \;& -ik_0Y_0(\epsilon(x,y)-1)\{e^{ik_0\sin\phi_0 x}[e^{-ik_0\cos\phi_0 y} + R_E(\phi_0)e^{ik_0\cos\phi_0 y}]\\
&+\textstyle\int_0^t\int_{-L/2}^{+L/2} J_z(x',y')G^p_{zz}(x,y;x',y')\mathrm{d}x'\mathrm{d}y'\},\\
J_x(x,y) = \;& -ik_0Y_0(\epsilon(x,y)-1)\{\cos\phi_0 e^{ik_0\sin\phi_0 x}[-e^{-ik_0\cos\phi_0 y} + R_H(\phi_0)e^{ik_0\cos\phi_0 y}]\\
&+\textstyle\int_0^t\int_{-L/2}^{+L/2}[J_x(x',y')G^p_{xx}(x,y;x',y') + J_y(x',y')G^p_{xy}(x,y;x',y')]\mathrm{d}x'\mathrm{d}y'\},\\
J_y(x,y) = \;& -ik_0Y_0(\epsilon(x,y)-1)\{-\sin\phi_0 e^{ik_0\sin\phi_0 x}[e^{-ik_0\cos\phi_0 y} + R_H(\phi_0)e^{ik_0\cos\phi_0 y}]\\
&+\textstyle\int_0^t\int_{-L/2}^{+L/2}[J_x(x',y')G^p_{yx}(x,y;x',y') + J_y(x',y')G^p_{yy}(x,y;x',y')]\mathrm{d}x'\mathrm{d}y'\}.
\end{aligned} \tag{20}$$

Far away from the surface ($y \gg \lambda_0$), contribution of only a few terms of the summations in (19) are observable. These terms correspond to values of n such that k_{ny} is real and they are known as the Bragg modes (see (16)). At low frequencies ($L < \lambda$) among all the Bragg modes the mode corresponding to $n = 0$ carries most of the scattered energy. The scattered field due to this mode is a plane wave and for E and H Polarization, respectively, we have

$$\begin{aligned}
\boldsymbol{E}_E = \;& \tfrac{-Z_0}{2L\cos\phi_0}\{\textstyle\int_0^t\int_{-L/2}^{+L/2} J_z(x',y')[e^{-ik_0\cos\phi_0 y'} + R_E e^{ik_0\cos\phi_0 y'}]e^{-ik_0\sin\phi_0 x'}\mathrm{d}x'\mathrm{d}y'\}\\
&\cdot e^{ik_0(\cos\phi_0 y + \sin\phi_0 x)}\hat{z}
\end{aligned} \tag{21}$$

$$\begin{aligned}
\boldsymbol{E}_H = \;& -\tfrac{Z_0}{2L\cos\phi_0}\{\cos\phi_0\textstyle\int_0^t\int_{-L/2}^{+L/2} J_x(x',y')[e^{-ik_0\cos\phi_0 y'} - R_H e^{ik_0\cos\phi_0 y'}]e^{-ik_0\sin\phi_0 x'}\mathrm{d}x'\mathrm{d}y'\\
&-\sin\phi_0\textstyle\int_0^t\int_{-L/2}^{+L/2} J_y(x',y')[e^{-ik_0\cos\phi_0 y'} + R_H e^{ik_0\cos\phi_0 y'}]e^{-ik_0\sin\phi_0 x'}\mathrm{d}x'\mathrm{d}y'\}\\
&\cdot(\cos\phi_0\hat{x} - \sin\phi_0\hat{y})e^{ik_0(\cos\phi_0 y + \sin\phi_0 x)}
\end{aligned} \tag{22}$$

5 Numerical Implementation

It is very unlikely to find analytical solutions to the equations given by (20) even for the simplest form of $\epsilon(x, y)$. However an approximate numerical solution can be obtained using the standard moment method with point matching technique. In this method the cross section of the inhomogeneous layer over one period is discretized into small rectangular segments over which the dielectric constant and polarization current can be assumed to be constant. Now in equation (20) the integrals over one period of the inhomogeneous layer can be broken up into summation of integrals over each segment where the polarization current is constant.

Let pq designate a cell whose center coordinate is $(x_p, y_q) = (p\Delta x, q\Delta y)$, where p and q are some integers and Δx and Δy are dimensions of the rectangular segments. If the fields polarization currents as given by (20) are evaluated at the center of uv-cell (point matching) the integral equations can be cast into matrix equations. The matrices formed by this technique are known as the impedance matrices. The solution to this matrix equation gives the polarization current at the center of each segment.

After a simple integration of the periodic Green's functions over the area of pq-cell, it can be shown that the entries of the impedance matrix for E polarization (TM case) are of the form

$$Z(u,v;p,q) = \begin{cases} \frac{2ik_0^2}{L}(\epsilon(u,v)-1)\sum_{n=-\infty}^{+\infty}[e^{ik_{ny}|y_v-y_q|} + R_E(\gamma_n)e^{ik_{ny}(y_v+y_q)}]\frac{\sin(k_{ny}\Delta y/2)}{k_{nx}k_{ny}^2} \\ \quad \cdot \sin(k_{nx}\Delta x/2)e^{-ik_{nx}(x_u-x_p)} & v \neq q \\ \frac{2ik_0^2}{L}(\epsilon(u,v)-1)\sum_{n=-\infty}^{+\infty}[-ie^{ik_{ny}\Delta y/2} + i + R_E(\gamma_n)e^{i2k_{ny}y_v} \\ \quad \cdot \sin(k_{ny}\Delta y/2)]\frac{1}{k_{nx}k_{ny}^2}\sin(k_{nx}\Delta x/2)e^{-ik_{nx}(x_u-x_p)} & v = q \ u \neq p \\ -1 + \frac{2ik_0^2}{L}(\epsilon(u,v)-1)\sum_{n=-\infty}^{+\infty}[-ie^{ik_{ny}\Delta y/2} + i + R_E(\gamma_n)e^{i2k_{ny}y_v} \\ \quad \cdot \sin(k_{ny}\Delta y/2)]\frac{1}{k_{nx}k_{ny}^2}\cdot\sin(k_{nx}\Delta x/2) & v = q \ u = p. \end{cases} \tag{23}$$

For H polarization (TE case) the integral equations for J_x and J_y are coupled, which result in coupled matrix equations that can be combined into a single matrix equation. The resultant impedance matrix consists of four sub-matrices of the following form

$$\mathcal{Z} = \begin{bmatrix} \mathcal{Z}_1 & \mathcal{Z}_2 \\ \mathcal{Z}_3 & \mathcal{Z}_4 \end{bmatrix},$$

whose entries are given by

$$Z_1(u,v;p,q)=\begin{cases}\frac{2ik_0^2}{L}(\epsilon(u,v)-1)\sum_{n=-\infty}^{+\infty}[e^{ik_{ny}|y_v-y_q|}-R_H(\gamma_n)e^{ik_{ny}(y_v+y_q)}]\frac{(1-k_{nx}^2/k_0^2)}{k_{nx}k_{ny}^2}\\ \quad\cdot\sin(k_{ny}\Delta y/2)\sin(k_{nx}\Delta x/2)e^{-ik_{nx}(x_u-x_p)} & v\neq q\\ \frac{2ik_0^2}{L}(\epsilon(u,v)-1)\sum_{n=-\infty}^{+\infty}[-ie^{ik_{ny}\Delta y/2}+i-R_H(\gamma_n)e^{i2k_{ny}y_v}\\ \quad\cdot\sin(k_{ny}\Delta y/2)]\frac{(1-k_{nx}^2/k_0^2)}{k_{nx}k_{ny}^2}\sin(k_{nx}\Delta x/2)e^{-ik_{nx}(x_u-x_p)}\\ & v=q\ u\neq p\\ -1+\frac{2ik_0^2}{L}(\epsilon(u,v)-1)\sum_{n=-\infty}^{+\infty}[-ie^{ik_{ny}\Delta y/2}+i-R_H(\gamma_n)e^{i2k_{ny}y_v}\\ \quad\cdot\sin(k_{ny}\Delta y/2)]\frac{(1-k_{nx}^2/k_0^2)}{k_{nx}k_{ny}^2}\cdot\sin(k_{nx}\Delta x/2) & v=q\ u=p,\end{cases}\tag{24}$$

$$Z_2(u,v;p,q)=\begin{cases}\frac{2i}{L}(\epsilon(u,v)-1)\sum_{n=-\infty}^{+\infty}[\mathrm{sgn}(y_v-y_q)e^{ik_{ny}|y_v-y_q|}+R_H(\gamma_n)e^{ik_{ny}(y_v+y_q)}]\\ \quad\cdot\frac{1}{k_{ny}}\sin(k_{ny}\Delta y/2)\sin(k_{nx}\Delta x/2)e^{-ik_{nx}(x_u-x_p)} & v\neq q\\ \frac{2i}{L}(\epsilon(u,v)-1)\sum_{n=-\infty}^{+\infty}R_H(\gamma_n)e^{i2k_{ny}y_v}\sin(k_{ny}\Delta y/2)\frac{1}{k_{ny}}\\ \quad\cdot\sin(k_{nx}\Delta x/2)e^{-ik_{nx}(x_u-x_p)} & v=q,\end{cases}\tag{25}$$

$$Z_3(u,v;p,q)=\begin{cases}\frac{2i}{L}(\epsilon(u,v)-1)\sum_{n=-\infty}^{+\infty}[\mathrm{sgn}(y_v-y_q)e^{ik_{ny}|y_v-y_q|}-R_H(\gamma_n)e^{ik_{ny}(y_v+y_q)}]\\ \quad\cdot\frac{1}{k_{ny}}\sin(k_{ny}\Delta y/2)\sin(k_{nx}\Delta x/2)e^{-ik_{nx}(x_u-x_p)} & v\neq q\\ \frac{2i}{L}(\epsilon(u,v)-1)\sum_{n=-\infty}^{+\infty}-R_H(\gamma_n)e^{i2k_{ny}y_v}\sin(k_{ny}\Delta y/2)\frac{1}{k_{ny}}\\ \quad\cdot\sin(k_{nx}\Delta x/2)e^{-ik_{nx}(x_u-x_p)} & v=q,\end{cases}\tag{26}$$

$$Z_4(u,v;p,q)=\begin{cases}\frac{2ik_0^2}{L}(\epsilon(u,v)-1)\sum_{n=-\infty}^{+\infty}\{(1-\frac{k_{ny}^2}{k_0^2})[e^{ik_{ny}|y_v-y_q|}+R_H(\gamma_n)e^{ik_{ny}(y_v+y_q)}]\\ \quad\frac{1}{k_{nx}k_{ny}^2}\cdot\sin(k_{ny}\Delta y/2)\sin(k_{nx}\Delta x/2)e^{-ik_{nx}(x_u-x_p)}\} & v\neq q\\ \frac{2ik_0^2}{L}(\epsilon(u,v)-1)\sum_{n=-\infty}^{+\infty}[-i(1-\frac{k_{ny}^2}{k_0^2})e^{ik_{ny}\Delta y/2}+i+R_H(\gamma_n)(1-\frac{k_{ny}^2}{k_0^2})\\ \quad\cdot\sin(k_{ny}\Delta y/2)e^{i2k_{ny}y_v}]\frac{1}{k_{nx}k_{ny}^2}\sin(k_{nx}\Delta x/2)e^{-ik_{nx}(x_u-x_p)}\\ & v=q\ u\neq p\\ -1+\frac{2ik_0^2}{L}(\epsilon(u,v)-1)\sum_{n=-\infty}^{+\infty}[-i(1-\frac{k_{ny}^2}{k_0^2})e^{ik_{ny}\Delta y/2}+i+R_H(\gamma_n)\\ \quad\cdot(1-\frac{k_{ny}^2}{k_0^2})\sin(k_{ny}\Delta y/2)e^{i2k_{ny}y_v}]\frac{1}{k_{nx}k_{ny}^2}\sin(k_{nx}\Delta x/2)\\ & v=q\ u=p.\end{cases}\tag{27}$$

In (25) and (26) $\mathrm{sgn}(x)$ is the sign function defined by

$$\mathrm{sgn}(x)=\begin{cases}+1 & \text{if } x>0\\ -1 & \text{if } x<0.\end{cases}\tag{28}$$

All series in (25), (26), and (27) are exponentially convergent and thus the series can be truncated for relatively small n. This is also the case for (24) except for one term in the summand of the expressions corresponding to $v=q$. The convergence rate of

$$S=\sum_{n=-\infty}^{+\infty}i\frac{(1-k_{nx}^2/k_0^2)}{k_{nx}k_{ny}^2}\cdot\sin(k_{nx}\Delta x/2)e^{-ik_{nx}(x_u-x_p)}\tag{29}$$

is very poor and in order to improve the convergence rate the standard trick is to add and subtract a series whose summand is asymptotic to the original series. For large n

$$k_{nx} \approx \frac{2\pi n}{L} \qquad k_{ny} \approx i\frac{2\pi n}{L}$$

and the summand is approximated by

$$\frac{i}{k_0^2}\frac{L}{2\pi n}\sin(k_{nx}\Delta x/2)e^{-ik_{nx}(x_u-x_p)}$$

where the asymptotic forms for k_{nx} and k_{ny} are only used in the amplitude factor. It can be shown that

$$\sum_{n=-\infty,n\neq 0}^{+\infty}\frac{e^{in\alpha}}{n} = i\mathrm{sgn}(\alpha)(\pi - \mid \alpha \mid) \tag{30}$$

where α is a real number. By employing (30), a closed form for the asymptotic series (S_{app}) can be obtained and is given by

$$S_{app} = \begin{cases} \frac{L}{2k_0^2}e^{-ik_{nx}(x_u-x_p)}[sgn(x_p-x_u)(1-\frac{2|x_p-x_u|}{L})\sin(k_0\sin\phi_0\Delta x/2) & \\ \quad -\frac{i\Delta x}{L}\cos(k_0\sin\phi_0\Delta x/2)] & x_p \neq x_u \\ \frac{iL}{2k_0^2}(1-\frac{\Delta x}{L})\cos(k_0\sin\phi_0\Delta x/2) & x_u = x_p \end{cases}$$

Now (29) can be written as

$$S = \frac{i}{k_0^2}\sum_{n=-\infty,n\neq 0}^{+\infty}[\frac{k_0^2-k_{nx}^2}{k_{nx}k_{ny}^2} - \frac{L}{2\pi n}]\sin(k_{nx}\Delta x/2)e^{-ik_{nx}(x_u-x_p)} + \frac{i\sin(k_0\sin\phi_0\Delta x/2)}{k_0^3\sin\phi_0} + S_{app}$$

in which case the series converges very fast.

The right-hand-side of the matrix equations may be represented by an excitation vector whose elements, for E polarization, are

$$b(u,v) = ik_0Y_0(\epsilon(x_u,y_v)-1)e^{ik_0\sin\phi_0x_u}[e^{-ik_0\cos\phi_0y_v} + R_E(\phi_0)e^{ik_0\cos\phi_0y_v}]$$

The excitation vector for H polarization is made up of two sub-vectors with entries

$$b_1(u,v) = ik_0Y_0(\epsilon(x_u,y_v)-1)\cos\phi_0e^{ik_0\sin\phi_0x_u}[-e^{-ik_0\cos\phi_0y_v} + R_H(\phi_0)e^{ik_0\cos\phi_0y_v}],$$
$$b_2(u,v) = -ik_0Y_0(\epsilon(x_u,y_v)-1)\sin\phi_0e^{ik_0\sin\phi_0x_u}[e^{-ik_0\cos\phi_0y_v} + R_H(\phi_0)e^{ik_0\cos\phi_0y_v}].$$

We point out that the inhomogeneous layer may have an arbitrary thickness profile with a maximum height t. In such cases we may assume that the layer has a constant thickness t and the permittivity corresponding to air-filled points is 1.

6 High Frequency Scattering from Stratified Cylinders

For dielectric cylinders with large radii of curvature, physical optics may be used to obtain the scattered field provided the dielectric has sufficient loss to prevent significant penetration through the cylinder (see Section 7.3). The dielectric loss also suppresses the effects of creeping waves which enhances the physical optics results. If the dielectric cylinder is stratified, the physical optics approximation could still be used if the radius of curvature of all the interface contours are much larger than the wavelength.

Two types of physical optics approximations can be applied: 1) surface integral and 2) volume integral approximation . In surface integral physical optics the equivalent surface currents are approximated by electric and magnetic surface currents of the infinite tangential plane. In the latter method the volumetric polarization current is estimated by finding the internal field using geometrical optics ray tracing. Of the two techniques, the surface integral physical optics is much easier to employ. The standard physical optics surface currents are given by (28) and (29). New physical optics surface currents that are more convenient to work with are examined. These currents can be obtained by noting that the reflected plane wave from a dielectric interface can be generated by equivalent electric and magnetic current sheets. These currents are normal to the plane of incidence and their density is proportional to the incident field amplitude, polarization, and associated Fresnel reflection coefficient. Suppose the incident field is given by (26) and the normal to the cylinder surface is represented by the unit vector $\hat{n}$. The unit vector normal to the plane of incidence is

$$\hat{t} = \frac{\hat{n} \times \hat{k}_i}{\mid \hat{n} \times \hat{k}_i \mid},$$

in terms of which the new physical optics electric and magnetic currents are given by

$$\boldsymbol{J}_e = -2Y_0(\boldsymbol{E}_0 \cdot \hat{t}) \cos\phi_i R_E(\phi_i) e^{ik_0 \hat{k}_i \cdot \boldsymbol{r}} \hat{t} \tag{31}$$

$$\boldsymbol{J}_m = -2Z_0(\boldsymbol{H}_0 \cdot \hat{t}) \cos\phi_i R_H(\phi_i) e^{ik_0 \hat{k}_i \cdot \boldsymbol{r}} \hat{t} \tag{32}$$

Here, R_E and R_H are Fresnel reflection coefficients and ϕ_i is the local angle of incidence given by

$$\phi_i = \arccos(-\hat{n} \cdot \hat{k}_i).$$

In shadow regions on the surface ($\phi_i > \pi/2$) the currents are zero.

Suppose a stratified cylinder with arbitrary cross section is illuminated by a plane wave travelling in $-x$ direction ($\hat{k}_i = -\hat{x}$) as shown in Fig. 5. The outer surface of the

cylinder is described by a smooth function $\rho(\phi)$. For E-polarized wave ($\boldsymbol{E}_0 = \hat{z}$) only electric current and for H-polarized wave ($\boldsymbol{H}_0 = Y_0\hat{z}$) only magnetic current is induced on the cylinder surface as given by (31) and (32). It can easily be shown that in the far zone of the cylinder in a direction denoted by ϕ_s, the far field amplitudes for E and H polarization respectively are given by

$$\boldsymbol{S}_E = \hat{z}\frac{k_0}{2}\int_{\text{lit}} \cos\phi_i R_E(\phi_i) e^{-ik_0\rho(\phi')(\cos\phi' + \cos(\phi' - \phi_s))}\sqrt{\rho^2(\phi') + \rho'^2(\phi')}\mathrm{d}\phi' \tag{33}$$

$$\boldsymbol{S}_H = \hat{\phi}\frac{k_0}{2}\int_{\text{lit}} \cos\phi_i R_H(\phi_i) e^{-ik_0\rho(\phi')(\cos\phi' + \cos(\phi' - \phi_s))}\sqrt{\rho^2(\phi') + \rho'^2(\phi')}\mathrm{d}\phi' \tag{34}$$

where the integral is taken over the lit region and ρ' is the derivative of ρ with respect to ϕ. If the surface of the cylinder is convex the integral in (33) and (34) can be evaluated

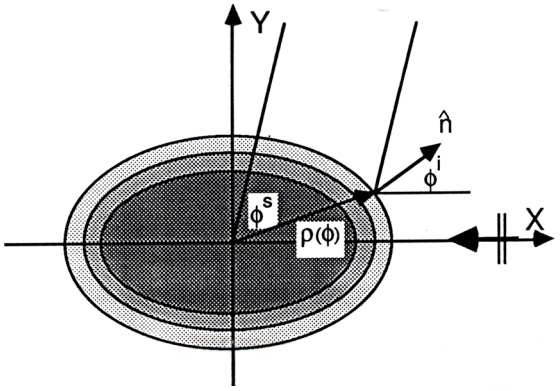

Figure 5: Geometry of scattering problem of a stratified cylinder.

using the stationary phase technique. The stationary point (ϕ_{SP}) is the root of the equation

$$\frac{\mathrm{d}}{\mathrm{d}\phi'}\rho(\phi')\left(\cos\phi' + \cos(\phi' - \phi_s)\right) = 0.$$

By noting that at the stationary point $\phi_i = \phi_s/2$ and

$$\sqrt{\rho^2(\phi') + \rho'^2(\phi')} = \frac{\rho(\phi_{SP})}{\cos(\phi_{SP} - \phi_s/2)},$$

and also by defining

$$g = \frac{\mathrm{d}^2}{\mathrm{d}\phi'^2}[\rho(\phi')\left(\cos\phi' + \cos(\phi' - \phi_s)\right)]_{\phi'=\phi_{SP}}$$

equations (33) and (34) become

$$\boldsymbol{S}_E = \hat{z}\cos(\frac{\phi_s}{2})R_E(\frac{\phi_s}{2})\frac{\rho(\phi_{SP})}{\cos(\phi_{SP}-\phi_s/2)}\sqrt{\frac{k_0\pi}{2\mid g\mid}}e^{-ik_0\rho(\phi_{SP})(\cos\phi_{SP}+\cos(\phi_{SP}-\phi_s))} \cdot e^{-i\mathrm{sgn}(g)\frac{\pi}{4}}\ , \tag{35}$$

$$\boldsymbol{S}_H = \hat{\phi}\cos(\frac{\phi_s}{2})R_H(\frac{\phi_s}{2})\frac{\rho(\phi_{SP})}{\cos(\phi_{SP}-\phi_s/2)}\sqrt{\frac{k_0\pi}{2\mid g\mid}}e^{-ik_0\rho(\phi_{SP})(\cos\phi_{SP}+\cos(\phi_{SP}-\phi_s))} \cdot e^{-i\mathrm{sgn}(g)\frac{\pi}{4}}\ . \tag{36}$$

For a circular cylinder of radius a these expressions simplify to

$$\boldsymbol{S}_E = \hat{z}\frac{1}{2}\sqrt{k_0\pi a\cos(\phi_s/2)}R_E(\frac{\phi_s}{2})e^{-i2k_0a\cos(\phi_s/2)}e^{i\pi/4} \tag{37}$$

$$\boldsymbol{S}_H = \hat{\phi}\frac{1}{2}\sqrt{k_0\pi a\cos(\phi_s/2)a}R_H(\frac{\phi_s}{2})e^{-i2k_0a\cos(\phi_s/2)}e^{i\pi/4} \tag{38}$$

To verify the validity of the physical optics expressions with new set of physical optics currents we compare expressions (37) and (38) for a layered circular cylinder with the exact series solution [Ruck et al, 1970, pp. 259]. Let us consider a two-layer cylinder with inner and outer radii of $a_1 = 10cm$ and $a = 10.5cm$ respectively. The dielectric constant of the inner and outer layers respectively are $15+i7$ and $4+i1$. These values are so chosen to simulate a tree with smooth bark. Figures 6 and 7 compare the normalized backscattering cross section ($\sigma/\pi a$) of the cylinder for E and H polarizations using physical optics expressions and exact series solution. In these figures the cross section of the cylinder in absence of the outer layer (bark) is also plotted to demonstrate the effect of the bark on reducing the cross section of the cylinder. For frequencies above 2 GHz ($k_0a = 4.2$) the agreement between the two solution is excellent. The bark layer plays the role of an impedance transformer which reduces the cross section of the cylinder by 14 dB around $k_0a = 16$.

7 Scattering from Corrugated Cylinder

Consider a corrugated dielectric cylinder with arbitrary cross section as shown in Fig. 8. Assume the corrugation geometry is such that the humps are identical and of equal distance L from each other. Further assume that if the corrugation is removed the surface of the cylinder would be denoted as before by $\rho(\phi)$ and the radius of curvature at each point is much larger than the wavelength and L. Under these conditions each point on the cylinder surface can be replaced, approximately, by a periodic corrugated surface. The accuracy of this approximation is in the order of physical optics approximation for smooth cylinders.

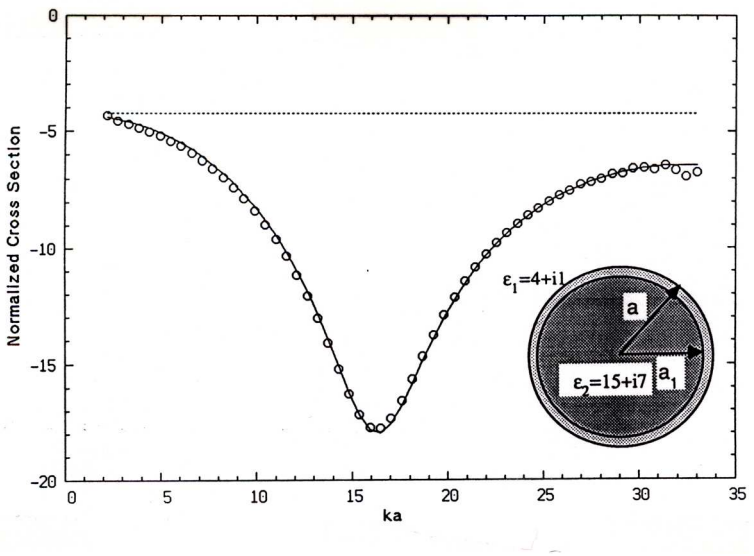

Figure 6: Normalized backscattering cross section ($\frac{\sigma}{\pi a}$) of a two-layer dielectric cylinder with $a = 10.5cm$, $a_1 = 10cm$, $\epsilon_1 = 15 + i7$, $\epsilon_2 = 4 + i1$ versus $k_0 a$ for TM case: (——) physical optics solution, (o o o) exact solution, (- - -) physical optics solution for homogeneous cylinder $a = 10.5cm$ $\epsilon = 15 + i7$.

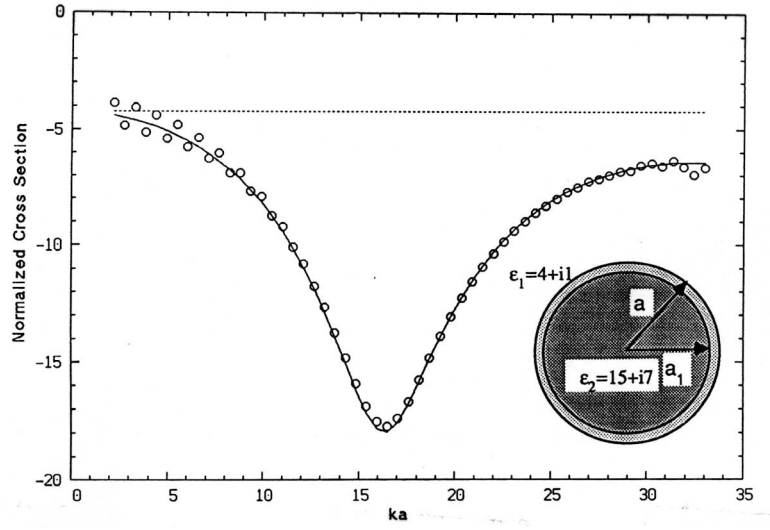

Figure 7: Normalized backscattering cross section ($\frac{\sigma}{\pi a}$) of a two-layer dielectric cylinder with $a = 10.5cm$, $a_1 = 10cm$, $\epsilon_1 = 15 + i7$, $\epsilon_2 = 4 + i1$ versus $k_0 a$ for TE case: (— –) physical optics solution, (o o o) exact solution, (- - -) physical optics solution for homogeneous cylinder $a = 10.5cm$ $\epsilon = 15 + i7$.

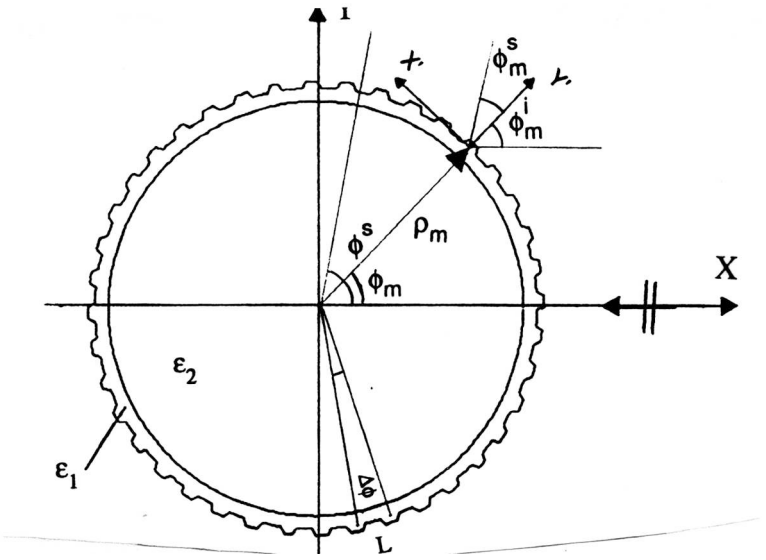

Figure 8: A corrugated cylinder geometry.

Suppose the cylinder is illuminated by a plane wave travelling in $-x$ direction and let us denote the tangential coordinate at the center of each hump by (x', y') where $\hat{y'}$ coincides with the outward normal unit vector $(\hat{n}(\phi))$. If the origin of the prime coordinate system corresponding to the m^{th} hump is located at (ρ_m, ϕ_m) we have

$$\phi_m = \sum_{\ell=1}^{m} \Delta\phi_\ell - \frac{\pi}{2}, \tag{39}$$

$$\Delta\phi_{\ell+1} = \frac{L}{\sqrt{\rho^2(\phi_\ell) + \rho'^2(\phi_\ell)}}, \tag{40}$$

where $\Delta\phi_1$ is a known quantity. The local incidence angle at the m^{th} hump can be obtained from

$$\phi_m^i = \arccos(\hat{n}(\phi_m) \cdot \hat{x})$$

and the induced current in the m^{th} hump can be approximated by that of the periodic corrugated surface when the incidence angle is ϕ_m^i. The scattering direction is denoted by ϕ_s as before and the scattering direction for the m^{th} local coordinate is given by

$$\phi_m^s = \phi_s - \phi_m^i.$$

The far field due to the m^{th} hump ($\boldsymbol{S}_m$), depending on the polarization, can be obtained from (10) and we note that those humps with $\mid \phi_m^s \mid > \pi/2$ do not contribute to the far field. The total contribution of the cylinder corrugation to the far field is the vector

sum of the fields due to each hump modified by a phase factor to correct for the relative positions of the humps. Therefore

$$\boldsymbol{S}_c = \sum_m \boldsymbol{S}_m e^{-ik_0 x_m} e^{-ik_0(x_m \cos\phi_s + y_m \sin\phi_s)}, \tag{41}$$

where

$$x_m = \rho_m \cos\phi_m,$$
$$y_m = \rho_m \sin\phi_m.$$

The total scattered field may now be obtained from

$$\boldsymbol{S} = \boldsymbol{S}_c + \boldsymbol{S}_s,$$

where $\boldsymbol{S}_s$ is the far field amplitude of the smooth cylinder.

8 Numerical Results

To examine the effect of surface corrugation on scattering from corrugated cylinders, we consider a two-layer circular cylinder with uniform corrugation. The pertinent parameters are chosen as follows: each hump is a $\lambda_0/8 \times \lambda_0/8$ square with dielectric constant $\epsilon_1 = 4+i1$, the distance between humps is $L = \lambda/4$, the thickness and dielectric constant of outer layer are $\lambda/2$ and $4+i1$ respectively, and the radius and the dielectric constant of inner layer are 10λ and $15+i7$ respectively. For the corresponding periodic surface all the components of the induced current in each hump are obtained by the moment method and the amplitude and phase of the total current ($\int_s J(x',y')\mathrm{d}x'\mathrm{d}y'$) are plotted in Figs. 9 and 10. Figures 11-14 show the amplitude and the phase of the zeroth Bragg mode as given in (21) and (22), the reflected wave in the absence of the corrugations, and the sum of the two waves (total reflected wave) as a function of incidence angle. For E polarization (Fig. 11) the total reflected wave is less than the reflected wave in the absence of corrugation (reduction in the scattered field). In this case, as far as the total reflected field is concerned, the corrugation can be replaced by a homogeneous dielectric layer with thickness $\lambda/8$ and $\epsilon = 2.6 + i0.58$. For H polarization (Fig. 13) the total reflected wave is weaker than the reflected wave in the absence of the corrugation for angles less than the Brewster angle and vice versa for angles greater than the Brewster angle.

Once the induced current versus angle is obtained the bistatic scattered field can be computed from (41). Figures 15 and 15 show the far field amplitude due to the corrugation (S_c) and smooth cylinder (S_s) and the total far field amplitude ($S_c + S_s$). To examine the role of the outer layer, the far field amplitude of the cylinder when the outer layer is removed is also plotted. It is seen that the smooth bark reduces the scattered field

by 3 dB and the corrugation on the bark further reduces the scattered field by another 8 dB. In Fig. 16 the total far field amplitude , for TM case, of the corrugated cylinder is compared with a smooth cylinder when corrugation is replaced by an equivalent layer (thickness=$\lambda/8$, $\epsilon = 2.6 + i0.58$). Excellent agreement is obtained.

9 Conclusions

A hybrid solution based on the moment method and physical optics approximation is obtained for corrugated layered cylinders. The only restriction on the physical dimensions is the radius of curvature (r) of the cylinder where we require $r \gg \lambda$. Also new physical optics expressions for the equivalent surface current on the dielectric structure is introduced. This method is employed to investigate the effect of bark and its roughness on the scattering from tree trunks and branches. It is shown that the bark and its roughness both reduce the radar cross section. The low contrast dielectric bark layer manifest its effect more significantly at higher frequencies where the bark thickness and its roughness are a considerable fraction of the wavelength. It is also demonstrated that the roughness of the bark can be replaced with a homogeneous layer for the TM case. This suggests the possibility of replacing the roughness with an anisotropic layer for the case of an arbitrary polarization.

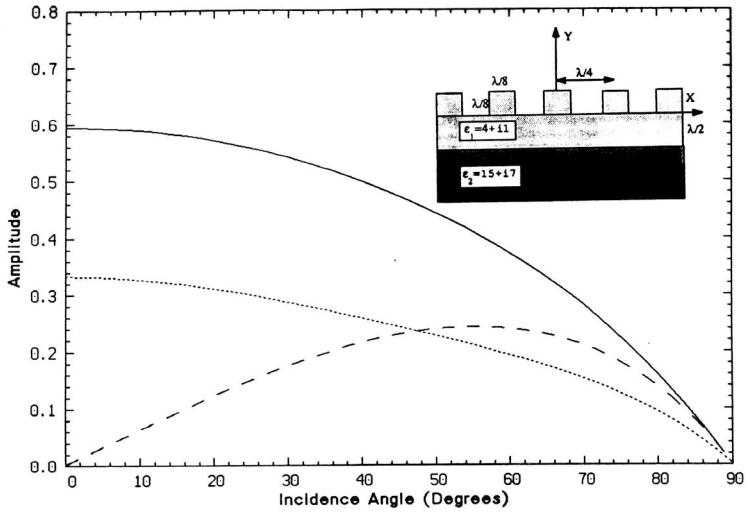

Figure 9: Amplitude of the total induced current in a two-layer periodic corrugated surface versus incidence angle: (——) z component of the current (E polarization), (- - -) x component of current and (– –) y component of the current (H polarization).

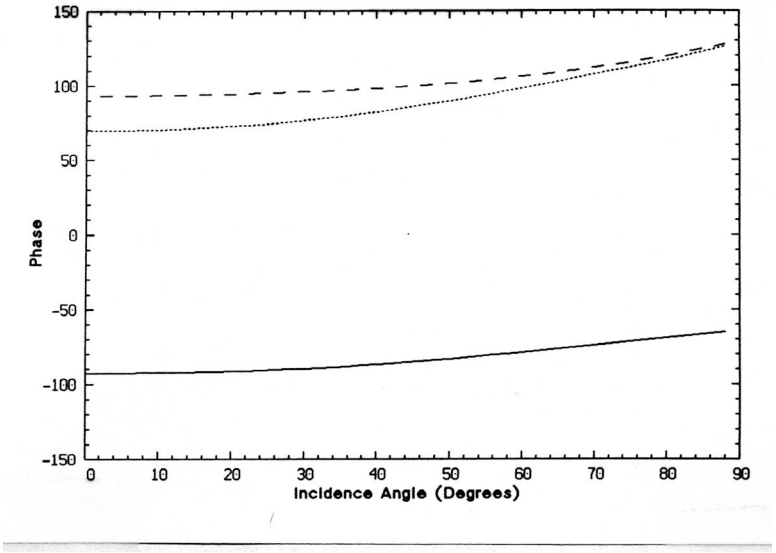

Figure 10: Phase of the total induced current in a two-layer periodic corrugated surface versus incidence angle: (——) z component of the current (E polarization), (- - -) x component of current and (– –) y component of the current (H polarization).

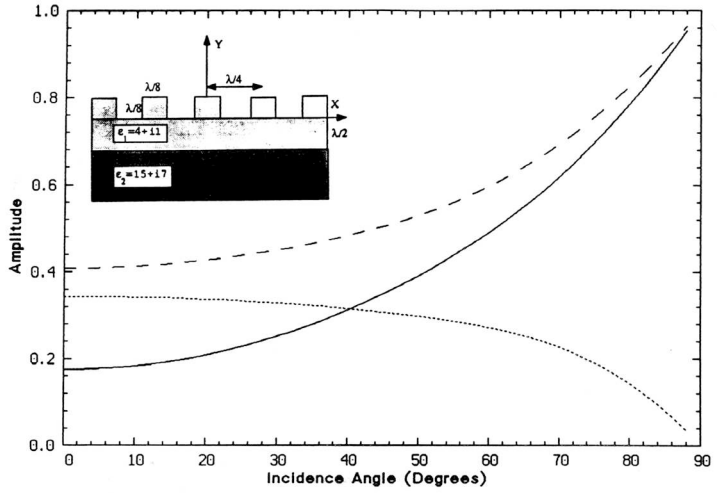

Figure 11: Amplitude of the reflected field from a two-layer periodic corrugated surface versus incidence angle for E polarization: (- - -) zeroth order Bragg mode, (– –) reflected field in absence of corrugation, (——) total reflected field.

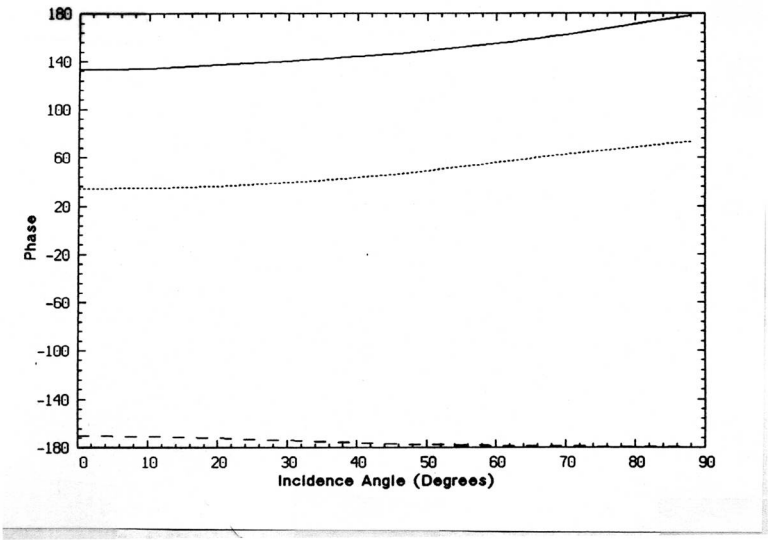

Figure 12: Phase of the reflected field from a two-layer periodic corrugated surface versus incidence angle for E polarization: (- - -) zeroth order Bragg mode, (– –) reflected field in absence of corrugation, (——) total reflected field.

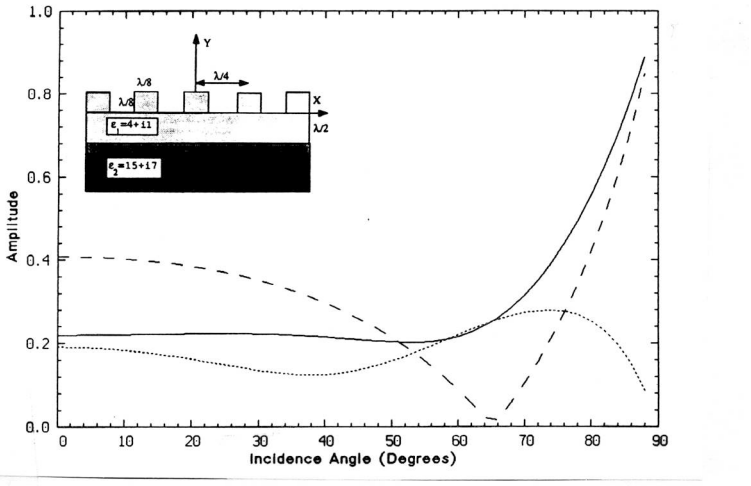

Figure 13: Amplitude of the reflected field from a two-layer periodic corrugated surface versus incidence angle for H polarization: (- - -) zeroth order Bragg mode, (– –) reflected field in absence of corrugation, (——) total reflected field.

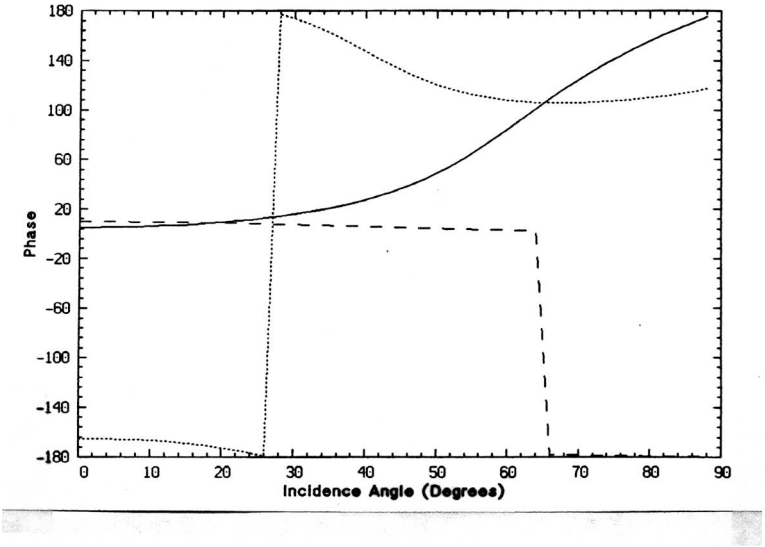

Figure 14: Phase of the reflected field from a two-layer periodic corrugated surface versus incidence angle for H polarization: (- - -) zeroth order Bragg mode, (– –) reflected field in absence of corrugation, (——) total reflected field.

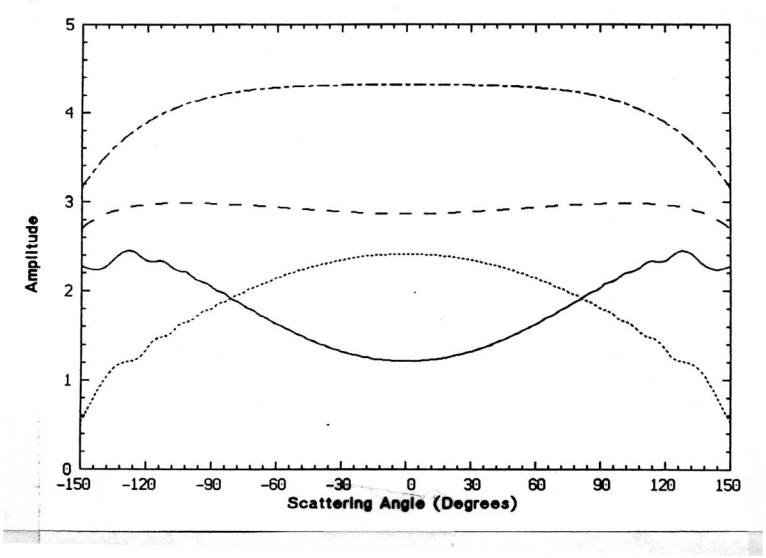

Figure 15: Far field amplitude of a corrugated cylinder for TM case with $a = 10.5\lambda_0$, $a_1 = 10\lambda_0$, $L = \lambda_0/4$, $\epsilon_1 = 4 + i1$, and $\epsilon_2 = 15 + i7$; (- - -) contribution of corrugation (S_c), (– –) contribution of smooth cylinder (S_s), (——) total far field amplitude ($S_s + S_c$), and (– - –) far field amplitude for smooth cylinder in absence of corrugation and outer layer.

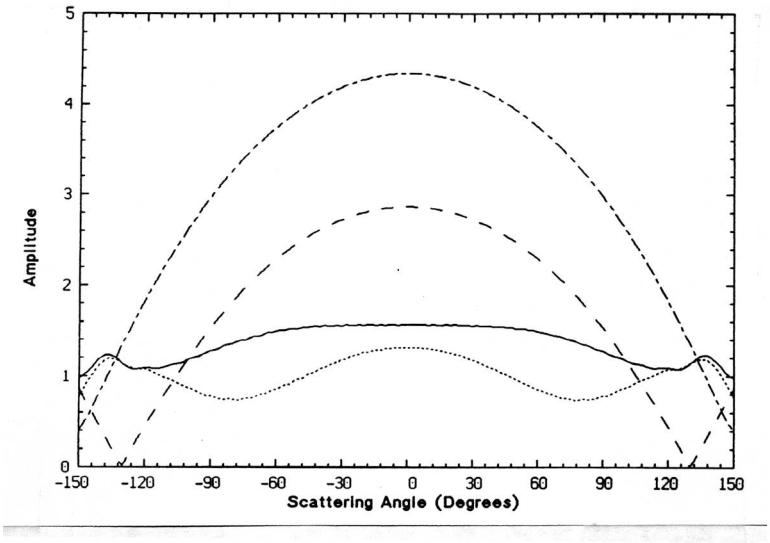

Figure 16: Far field amplitude of a corrugated cylinder for TE case with $a = 10.5\lambda_0$, $a_1 = 10\lambda_0$, $L = \lambda_0/4$, $\epsilon_1 = 4 + i1$, and $\epsilon_2 = 15 + i7$; (- - -) contribution of corrugation (S_c), (– –) contribution of smooth cylinder (S_s), (——) total far field amplitude ($S_s + S_c$), and (– - –) far field amplitude for smooth cylinder in absence of corrugation and outer layer.

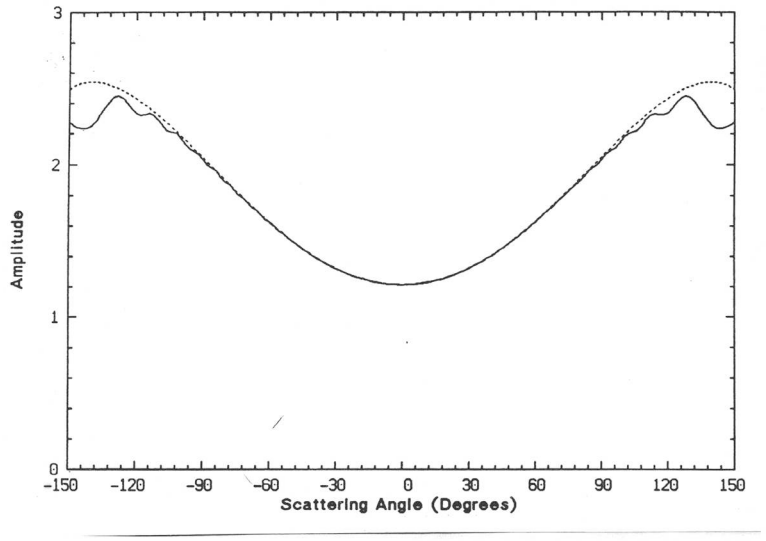

Figure 17: Far field amplitude of the corrugated cylinder (——) and equivalent three-layer cylinder (- - -) for TM case.